Molecular Crystals and Liquid Crystals
Publication details, including instructions for authors and subscription information:
http://www.tandfonline.com/loi/gmcl18

Electrically and Optically Controlled Light Modulation and Color Switching Using Helix Distortion of Ferroelectric Liquid Crystals

I. Abdulhalim [a] & G. Moddel [a]
[a] Department of Electrical and Computer Engineering and Center for Optoelectronic Computing Systems, University of Colorado, Boulder, CO, 80309-0425
Version of record first published: 04 Oct 2006.

To cite this article: I. Abdulhalim & G. Moddel (1991): Electrically and Optically Controlled Light Modulation and Color Switching Using Helix Distortion of Ferroelectric Liquid Crystals, Molecular Crystals and Liquid Crystals, 200:1, 79-101

To link to this article: http://dx.doi.org/10.1080/00268949108044233

Mol. Cryst. Liq. Cryst., 1991, Vol. 200, pp. 79–101
Reprints available directly from the publisher
Photocopying permitted by license only

Printed in the United States of America

Electrically and Optically Controlled Light Modulation and Color Switching Using Helix Distortion of Ferroelectric Liquid Crystals

I. ABDULHALIM and G. MODDEL

Department of Electrical and Computer Engineering and Center for Optoelectronic Computing Systems, University of Colorado, Boulder, CO 80309-0425

(Received September 18, 1990; in final form November 15, 1990)

The electro-optic effect associated with the helix distortion of chiral smectic C (SmC*) liquid crystals and its application to light modulation are investigated. Optically and electrically addressed spatial light modulators based on this effect are demonstrated. They exhibit an analog response, response times as short as 100 μs, good contrast ratio and resolution, and color switching capability. The analog response is shown to be a result of the gradual distortion of the helix at low voltages. Optically this corresponds to a linear rotation of the average optic axis and change of the average effective birefringence. From measurements of the wavelength of the maximum transmission the birefringence has been found to change as a function of dc voltage and frequency of ac voltage and magnitude. The agreement between theory and experiment suggests that color changes are due solely to birefringence changes associated with changes in the geometry of the helix. We derive expressions for the angle of rotation α of the average optic axis and birefringence Δn_{av} for the case of small distortions. It is shown that α varies linearly with field in this regime while Δn_{av} varies quadratically. The rotation of the average optic axis is shown to be in a plane.

Keywords: ferroelectric liquid crystals, light modulation, spatial light modulators, distorted helix, color switching

I. INTRODUCTION

Chiral smectic liquid crystals exhibit several electro-optic effects which make them useful for high speed spatial light modulators.[1] A spatial light modulator (SLM) is a device which can modulate one or two dimensional optical beams. It may be electrically or optically addressed, i.e. the modulation of an incoming light beam can be controlled either by applying an electrical signal or an optical signal. Interest in optically addressed spatial light modulators (OASLMs) has grown recently because of their importance in optical computing, optical signal processing and projection displays.[2]

The best known SLM utilizing chiral smectic liquid crystals (LC) is based on the surface stabilization[3] of the helix of the SmC* phase (SSFLC-SLM). It switches

with response times in the 100 μs range (100 times shorter than nematic SLMs), exhibits memory effects, the possibility of binary response, high contrast ratio and resolution[4] as high as 100 lp/mm.

The electroclinic effect in the chiral smectic A phase (SmA*) allows for higher speed SLMs down to submicroseconds, depending on the liquid crystal mixture and temperature[5,6] and has an analog response.[7] The available electroclinic LC mixtures, however, exhibit poor modulation and usually operate above room temperature.

The fact that an applied electric field parallel to the smectic layers distorts the helix of SmC* LC in its helicoidal geometry has been known since the early days[8] of ferroelectric LCs. The electro-optic effects associated with this distortion were studied by different investigators,[9,10] but their application to SLMs was not fully demonstrated. The first OASLM based on the distorted helix ferroelectric mode of operation (DHF) was reported by Beresnev *et al.*[10] Their published data includes only a photograph of an image imprinted on the device under dc bias after prolonged exposure to light. Considerable attention has recently[11–14] been devoted to the DHF mode of operation since several LC mixtures which possess a helicoidal pitch shorter than 1 μm at room temperature have been synthesized.

In a previous short technical paper[14] we reported an OASLM based on the DHF mode incorporating hydrogenated amorphous silicon p-i-n photodiode as the photosensor. We have shown that the DHF-OASLM exhibits analog response with good contrast ratio and resolution. In addition the DHF-SLM has a color selecting capability which together with the grey levels make it useful for full color displays. A more detailed study of the transfer characteristics of DHF-OASLMs will be published elsewhere.[15] In this work we concentrate on the physics of these devices and analyze the transfer characteristics and the color switching capability of both electrically and optically addressed DHF-SLMs. In section II we describe the geometry and the effect of an applied electric field on the helix. In section III we describe the electro-optic effects associated with the helix distortion and derive approximate analytic expressions for the angle of rotation of the optic axis and the changes in the birefringence. In Section IV we describe the experimental procedure for preparing the SLMs and the technique for measuring their response. Results showing the main transfer characteristics are presented and analyzed. In Sections VII and VIII we give detailed experimental and theoretical studies of the color-selecting capability.

II. GEOMETRY AND THE EFFECT OF AN ELECTRIC FIELD ON THE HELIX

The structure of SmC* LCs is layered where the molecular director in each layer is tilted by an angle θ with respect to the layers normal z. This tilt direction precesses due to the molecular chirality around the layers normal forming a helicoidal structure with pitch l_0. For a large electro-optic effect the geometry is usually planar where the layers are perpendicular to two glass substrates coated with transparent electrodes, above and below the LC (Figure 1). In the absence of an electric field,

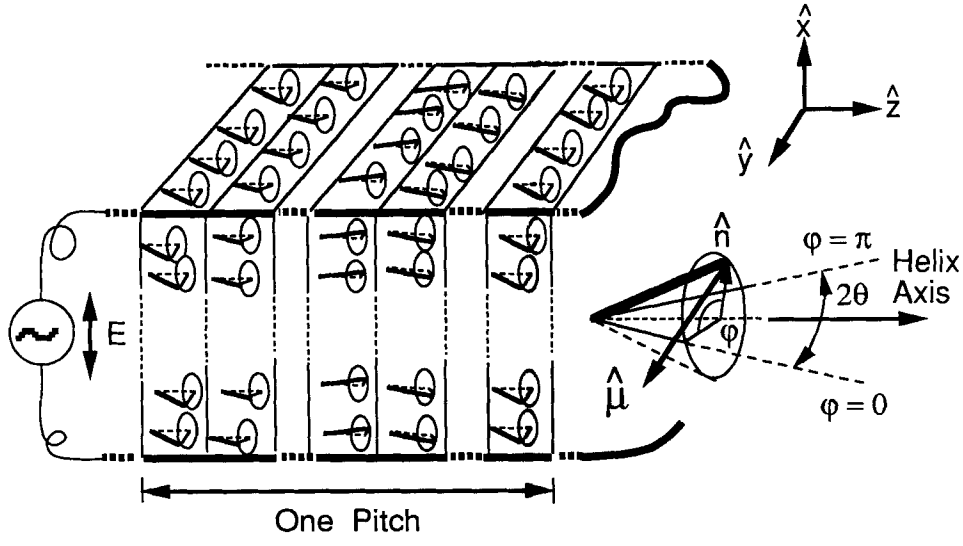

FIGURE 1 Geometry of the helicoidal structure showing one period of the helix with the layers perpendicular to two glass substrates coated with transparent oxide electrodes between which a field is applied.

the azimuth φ varies linearly with the coordinate z perpendicular to the layers: $\varphi = q_0 z$ with $q_0 = 2\pi/l_0$. The helix axis is along z. From symmetry considerations,[8] if the molecules possess a transverse dipole moment $\vec{\mu}$ then a net polarization density P_l within each layer appears. However since P_l precesses linearly around z it averages macroscopically to zero.

When an electric field E is applied parallel to the smectic layers it couples to the ferroelectric polarization in first order and to the static dielectric tensor in second order. The ferroelectric coupling will cause P_l to align parallel to E, that is the molecules perpendicular to E. The dielectric coupling becomes important at high fields where it causes the molecules to align parallel to E for positive dielectric anisotropy ($\Delta\varepsilon > 0$) and perpendicular to the field for $\Delta\varepsilon < 0$. Since most of the ferroelectric LC mixtures possess $\Delta\varepsilon < 0$, we assume this to be the case throughout the paper.

As a result of the coupling the helix distorts such that the molecules tend to align perpendicular to E. Opposing this tendency is the elastic force which tends to keep the layers in their equilibrium, nondistorted configurations, resulting in a complicated profile for $\varphi(z)$. Therefore the first molecules that align perpendicular to E are those in the layers near to the planes where $\varphi = \pi, 3\pi, 5\pi, \ldots$, for $E > 0$, and near to the planes where $\varphi = 0, 2\pi, 4\pi, \ldots$, for $E < 0$. As $|E|$ increases, the number of planes, and hence the size, of the regions where φ is an odd multiple of π for $E > 0$ and where φ is an even multiple of π for $E < 0$ increases. The size of the regions between the above planes decreases forming walls with thickness $\xi = (k_e/P_l E)^{1/2}$ where k_e is an effective elastic constant. The annihilation of these walls proceeds via solitary wave motion at large fields. The behavior of the helicoidal pitch with E is such that it increases gradually with E until a critical field

E_c where it diverges and the helix is unwound. In the unwound states all the molecules are oriented in the $\varphi = 0$ or $\varphi = \pi$ states, depending on the sign of E.

For a more quantitative description of the helix distortion, it is convenient to write the dynamic equation governing the motion of the azimuth angle φ given by the double sine-Gordon equation:

$$\eta_\varphi \frac{\partial \varphi}{\partial t} = k_e \frac{\partial^2 \varphi}{\partial z^2} \pm P_l E \sin\varphi + \left(\frac{\Delta\varepsilon E^2}{8\pi}\right) \sin 2\varphi \tag{1}$$

Here the left-hand side represents the viscoelastic torque and the right-hand side terms are the elastic, ferroelectric and dielectric torques respectively. η_φ is the orientational viscosity associated with φ motion, $\Delta\varepsilon = \varepsilon_3 \sin^2\theta + \varepsilon_1 \cos^2\theta - \varepsilon_2$, is the dielectric anisotropy where ε_1, ε_2 and ε_3 are the principal static dielectric constants. k_e is an effective elastic constant given by $k_e = \sin^2\theta\,(k_t \sin^2\theta + k_b \cos^2\theta)$ where k_t and k_b are the twist and bend elastic constants. The "+" sign corresponds to a field-induced "UP" orientation ($\varphi = \pi$) and the "−" a "DOWN" orientation ($\varphi = 0$). In Equation 1 variations in the tilt angle, inertial terms, flexoelectric terms and the self field of the ferroelectric polarization are neglected. The justification for these approximations is discussed elsewhere.[16]

There are no analytic solutions to Equation 1, but numerical integrations were performed recently[17] and revealed many interesting features of the switching mechanism. It is possible to express approximate solutions to Equation 1 for the case of small fields in analytic forms. For the description of the electro-optic effects these solutions are adequate, as will be shown in the following sections.

A convenient approximation to Equation 1 is to neglect the dielectric coupling term compared to the ferroelectric term. This approximation is valid because the dielectric coupling term is typically smaller by a factor of 10–15 than the ferroelectric term even for fields very close to E_c. In this case the steady state solution is known in terms of elliptic integrals.[18,19] Time dependent analytic solutions exists only for the case of small fields. For a small time dependent field like $E(t) = E\cos(\omega t)$, the solution may be expanded to series and taking only the first order:

$$\varphi(z, t) = q_0 z + \delta\varphi \tag{2}$$

Let $\delta\varphi$ has the following space and time dependence: $\delta\varphi = a(t)\sin q_0 z$ with $a(t)$ as a small time dependent parameter. Inserting Equation 2 into Equation 1 and neglecting nonlinear terms of $a(t)$ we get:

$$a(t) = \frac{a_0}{1 + \left(\frac{\omega}{\omega_c}\right)^2}\left(\cos\omega t + \frac{\omega}{\omega_c}\sin\omega t - \exp(-\omega_c t)\right) \tag{3}$$

where $a_0 = (\pi^2/16)(E/E_c)$, and $E_c = (\pi^2/16)(k_e q_0^2/P_l)$ is the unwinding field at zero frequency, and $\omega_c = k_e q_0^2/\eta_\varphi$ is a characteristic frequency. In this approximation the switching time $\tau \sim 1/\omega_c$ is the elastic relaxation time independent of the applied field. We will discuss the behavior of the switching speed further in section VI.

III. ELECTRO-OPTIC EFFECTS ASSOCIATED WITH THE HELIX DISTORTION

III.1 General Considerations

Light propagating perpendicular to the helix of a SmC* LC medium exhibits unique properties different from the case of propagation along the helix or at a small angle to it.[20] There are two main effects of the medium on the transmitted light: (1) the change of the polarization state and (2) diffraction. The first is a result of the optical anisotropy which can be described in terms of the orientation of the optic axis with respect to the incident-light polarization, and the birefringence. The diffraction is a result of the spatial periodicity of the dielectric tensor perpendicular to the propagation direction. The disinclination lines which exist in planar samples[21] also contribute to the diffraction. These lines give rise to dark stripes on the sample separated by half the helicoidal pitch when viewed under a microscope between crossed polarizers.

Since the structure in the direction perpendicular to the propagation direction is nonuniform different cases may be considered: (1) When the wavelength of incident light is much smaller than the helicoidal pitch l ($\lambda \ll l$). In this limit each ray of light does not "feel" the nonuniformity and the structure acts as a locally homogeneous anisotropic medium. The diffraction will be hardly seen because the diffracted spots are close to each other. However, since the practical cell thicknesses (d) are a few microns, for $\lambda \ll l$ the structure may fall into the regime of surface stabilization ($l \geq d$). (2) In the opposite limit of $\lambda \gg l$ the structure is strongly nonuniform but the light cannot resolve this nonuniformity. The diffracted spots in this case will be separated by large angles and might not be visible at all. Again for wavelengths in the visible range this requires l to be in the ultraviolet wavelength range or smaller. (3) In the intermediate regime $\lambda \sim l$, which is the most practical case, the diffraction will be seen easily and the transmitted light will show variation in its phase with the coordinate z.

In first approximation one might consider the phase variation in case (3) in terms of an average birefringence and average optic axis direction. This could be approached by dividing the structure into its molecular layers, which are considered as uniform uniaxial slabs. The dielectric tensor is constant within each layer at z but it is a function of z, so that each layer has a different effective birefringence and optic axis direction. The overall transmitted light will be the sum of the outputs from all these birefringent layers in one period of the helix, i.e., the spatial average of the output over one pitch.

For the geometry shown in Figure 2 the transmittance through a layer at z between two crossed polarizers when neglecting reflections from the boundaries, is given by:

$$T(z) = \sin^2\left(\frac{k_0 d}{2}\Delta n(z)\right) \sin^2(2[\Omega(z) + \beta]) \tag{4}$$

Here $k_0 = 2\pi/\lambda_0$ is the wavevector of the incident light, and β is the angle between

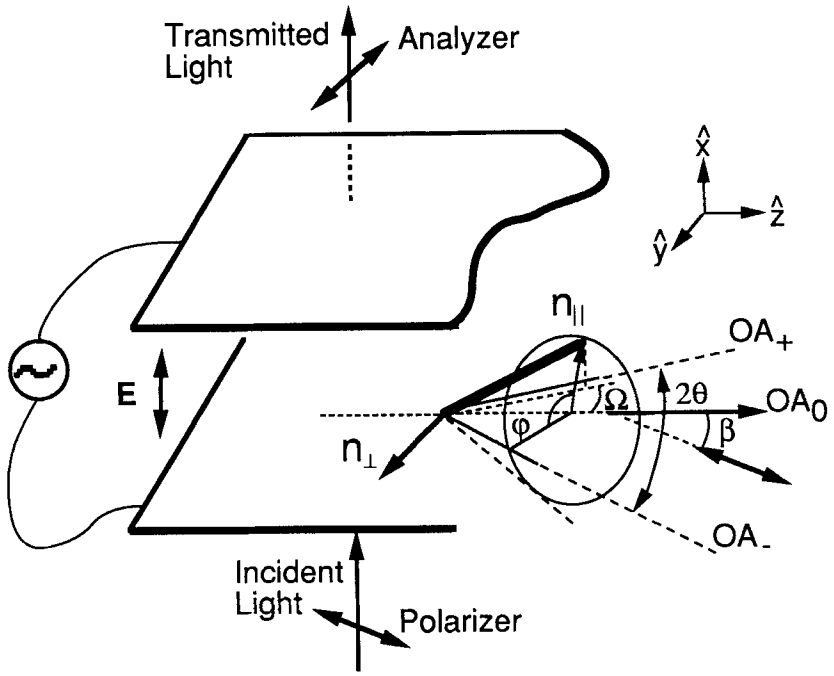

FIGURE 2 Schematic diagram describing the electro-optic effect of the structure of Figure 1 between crossed polarizers with the light propagating perpendicular to the helix. OA_0, OA_+, and OA_- represent the directions of the average optic axis at zero field state and at the two unwound states respectively.

the incident light polarization and the z axis. $\Omega(z)$ is the angle between the projection of the optic axis on the polarizer plane (yz) and the z axis, given by:

$$\Omega(z) = \arctan(\tan\theta \cos\varphi(z)) \tag{5}$$

and $\Delta n = n_e(z) - n_0$ is the effective birefringence where $n_0 = (\varepsilon_\perp)^{1/2}$ is the ordinary refractive index and $n_e(z)$ is the extraordinary refractive index given by:

$$n_e(z) = \left(\frac{\varepsilon_\perp \varepsilon_{||}}{\varepsilon_\perp + \delta\varepsilon \sin^2\theta \sin^2\varphi(z)}\right)^{1/2} \tag{6}$$

where $\delta\varepsilon = \varepsilon_{||} - \varepsilon_\perp$ is the optical dielectric anisotropy.

The overall transmittance will be the space average of $T(z)$ over one pitch. This approach was used by Ostrovsky *et al.*[9] and the average was performed numerically. The main assumption in this approach which is not justified is that one can consider the wavefields in each individual layer optically independent from those in the rest of the layers. Since the layer thickness is very small (20Å) compared to the wavelength of light, this cannot be justified. In our opinion it is physically more realistic to consider the LC medium in the average as uniaxial medium with a specified average birefringence and average optic axis direction. That is in calculating the transmittance we need to calculate the average of $\Delta n(z)$ and $\Omega(z)$ and insert them in Equation 4 rather than calculating the spatial average of the expression in Equation 4.

III.2 Average Birefringence and Optic Axis Direction

The dielectric tensor of the SmC* structure is a periodic function of the coordinate z. The average optic axis is determined by diagonalizing the average dielectric tensor and looking for the largest principal axis.

In terms of the azimuth angle φ the dielectric tensor $\tilde{\varepsilon}$ may be expressed as the following expansion:

$$\tilde{\varepsilon} = \sum_{n=-\infty}^{+\infty} \varepsilon_n \exp(i\varphi) \tag{7}$$

For the undistorted helix $\varphi = q_o z$ and Equation 7 is the Fourier expansion of $\tilde{\varepsilon}$. The matrix coefficients ε_n vanish for $|n| > 2$. The expressions for ε_n for the undistorted structure are given in different places.[20] The averaged $\tilde{\varepsilon}$ is therefore determined by the zero harmonic:

$$\tilde{\varepsilon}_{\text{avg}} = \begin{bmatrix} \varepsilon_\perp + \dfrac{\delta\varepsilon}{2}\sin^2\theta & 0 & 0 \\ 0 & \varepsilon_\perp + \dfrac{\delta\varepsilon}{2}\sin^2\theta & 0 \\ 0 & 0 & \varepsilon_\perp + \delta\varepsilon\cos^2\theta \end{bmatrix} \tag{8}$$

which shows that in the average the structure behaves as uniaxial medium with the average optic axis along the helix axis. The average birefringence is therefore given by:

$$\Delta n_{\text{avg}} = \sqrt{\varepsilon_\perp + \delta\varepsilon\cos^2\theta} - \sqrt{\varepsilon_\perp + \frac{\delta\varepsilon}{2}\sin^2\theta} \tag{9}$$

For the distorted helix, in general one needs to solve Equation 1 numerically and to perform the averaging of Equation 7. However, better insight can be gained by developing analytic solutions. Consider, for example, the solution given in Equation 2 for the case of small fields. The average dielectric tensor in this case (details of the calculation will be published elsewhere[21]) is given by:

$$\tilde{\varepsilon}_{\text{avg}} = \begin{bmatrix} \varepsilon_\perp + \dfrac{\delta\varepsilon}{2}\sin^2\theta(1 - J_{-1}(2a)) & 0 & 0 \\ 0 & \varepsilon_\perp + \dfrac{\delta\varepsilon}{2}\sin^2\theta(1 + J_{-2}(2a)) & \dfrac{-\delta\varepsilon}{2}\sin^2\theta J_{-1}(a) \\ 0 & \dfrac{-\delta\varepsilon}{2}\sin^2\theta J_{-1}(a) & \varepsilon_\perp + \delta\varepsilon\cos^2\theta \end{bmatrix} \tag{10}$$

where $J_{-1}(a)$ and $J_{-2}(2a)$ are Bessel functions of the first kind.

Diagonalizing $\tilde{\varepsilon}_{avg}$ in Equation 10 yields the following expression for the angle of rotation γ of the averaged optic axis in the yz plane:

$$\tan 2\gamma = \frac{-\tan(2\theta)J_{-1}(a)}{1 + \frac{\sin^2\theta}{2\cos 2\theta}(1 + J_{-2}(2a))} \tag{11}$$

since we are dealing with the case of small fields Equation 11 may be written as:

$$\tan 2\gamma = \frac{\pi^2 E(\cos \omega t + \frac{\omega}{\omega_c}\sin\omega t - \exp(-\omega_c t))}{32E_c[1 + \left(\frac{\omega}{\omega_c}\right)^2]}\tan 2\theta \tag{12}$$

Therefore γ varies linearly with E in this approximation. For an *ac* field the rotation decreases with the frequency and it suffers from a delay which depends on the frequency. Equation 12 shows that this approximation will hold only for rotation angles $\gamma < \theta/3$.

The birefringence seen by the light propagating along x axis is given by:

$$\Delta n_{avg} \approx \Delta n_m \left[1 - \frac{3}{2}\sin^2\theta + \frac{\sin^2 2\theta}{1 - \frac{3}{2}\sin^2\theta} J^2_{-1}(a)\right] \tag{13}$$

where $\Delta n_m = \sqrt{\varepsilon_\parallel} - \sqrt{\varepsilon_\perp}$ is the molecular birefringence. Equation 13 shows that Δn_{avg} does not depend on the sign of the field, which is expected because the optic axis rotates linearly with the field. The changes in the birefringence in this regime are small.

IV. EXPERIMENTAL

We performed experiments on different optically and electrically addressed devices with two different LC mixtures. The LC mixtures used were Chisso CS-1017 and Hoffman-La Roche FLC-6200. These materials exhibit the helicoidal smectic C structure in the temperature ranges $-20°$ to 55°C and $-3°$ to 59°C, and have room temperature helicoidal pitches of 0.8 μm and 0.37 μm, respectively. Therefore, no surface stabilization is expected in cells more than a few microns thick.[23] The cells were filled by capillary action, from the isotropic phase, between two transparent-electrode-coated glass plates having a sheet resistance of 14 ohms/square. For optically addressed devices one of these substrates is coated with *a*-Si:H as the photosensor. The deposition of *a*-Si:H photodiode in the *p-i-n* configuration has been described elsewhere.[4] Both surfaces were treated using a rubbed polymer

alignment technique. We prepared cells with different thicknesses using glass rods as spacers. The active area of the devices is a 12 mm diameter circle.

To check for the existence of the helicoidal structure we examined the samples under a polarizing microscope, looking for dark lines with a spacing equal to half the helicoidal pitch which corresponds to the distance of the disinclination lines.[21] For the CS-1017 LC mixture these dark lines exist in cells thicker than 4–5 μm, while for the FLC6200 LC mixture they were observed with thicknesses of 3 μm. This existence of the helicoidal structure was also supported by the diffraction pattern produced by these cells. Significant high spatial frequency diffraction was present in these cells under zero applied electric field. This diffraction pattern disappeared when a dc bias of ±1 to 3 volts was applied for cells with both mixtures, corresponding to the unwinding of the helix.

The optical response of an electrically addressed device was measured by a photodetector in transmission mode operation with the cell between crossed polarizers. The experimental setup for reflection mode operation of an OASLM has been described elsewhere.[4] To measure the optical response of the OASLM, we apply a square wave voltage between the two transparent electrodes. When the voltage is high (V+) and the *a*-Si:H photodiode is forward biased, nearly all of the applied voltage drops across the liquid crystal, switching it to one of the two unwound states (+). The cell is oriented such that the read beam polarization is either parallel or perpendicular to the projection of the optic axis in this state. The modulated read beam is partially reflected from the FLC/*a*-Si:H interface and extinguished by a crossed analyzer. This defines the OFF state.

When the voltage is negative (V−), most of the voltage drops across the reverse-biased photodiode; the LC remains OFF in the absence of write light. If a write light is present, photons absorbed by the *a*-Si:H produce electrical charges which charge the FLC to negative voltage and cause it to switch to the ON state. The rise time of the reflected read beam depends on both the magnitude of the photocurrent from the diode and the RC time constants associated with the constituent thin film layers. We used a collimated 514.5 nm beam from an Ar+ laser to write to the device.

Transient responses were measured using an expanded and collimated 632.28 nm read beam. The device output was focused onto a single photodetector. Color images were obtained by reading the device with a collimated white light source and imaging the output onto a CCD video camera. We also measured the spectral response of an electrically addressed cell using a Cary 219 spectrometer.

V. SLM RESPONSE

In Figure 3 we show oscilloscope traces of the response of an electrically addressed cell incorporating CS-1017 LC with a thickness of 5.6 μm. The upper trace shows the applied 200 Hz ac voltage. The bottom traces show the response of the device at different peak-to-peak voltages with increasing magnitude. The cell was rotated such that a minimum transmission was measured during the negative voltage interval. This figure demonstrates that the response resembles the shape of the ac

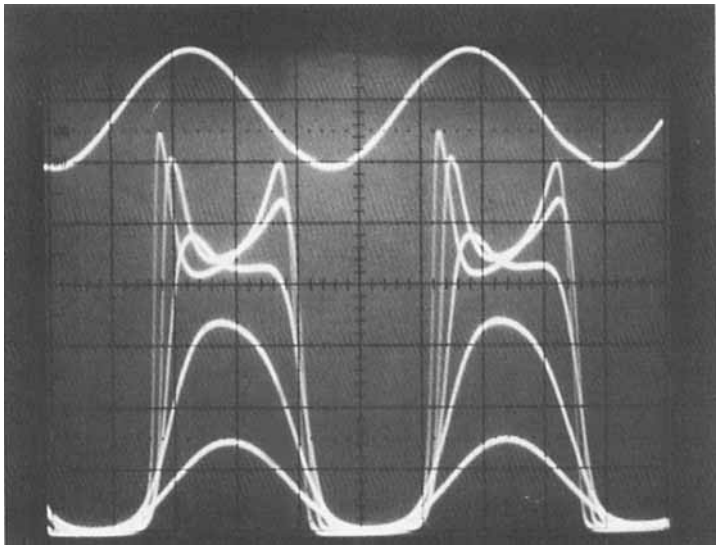

FIGURE 3 Oscilloscope traces to show the response of a 5.6 μm thick electrically addressed DHF-SLM made of CS-1017. The upper trace shows 200 Hz ac applied voltage. The lower traces show the transmitted read beam for the device in the geometry of Figure 2 for different peak-to-peak applied voltages in increasing magnitude from bottom to top as follows: 2, 5, 10, 20, and 30 volts.

wave for low applied voltages, indicating an analog response. For voltages higher than the unwinding voltage the transition to and from the ON state becomes very sharp, indicating a transition to a more binary type response. The unwinding voltage is a function of the frequency and for higher frequencies the response is analog over a wide range of voltages. The maximum contrast ratio from this cell is 200:1 and it is voltage dependent. The analog response at low voltages is a result of the gradual distortion of the helix yielding a linear voltage dependence of the angle of rotation of the optic axis, as was shown in Equation 12. The two peaks which appear at large voltages are due to two reasons. First, the tilt angle for CS-1017 LC is $\theta = 27°$ and the net optic axis rotation from one unwound state to the other is therefore $2\theta = 54°$. This causes the output to peak for times corresponding to a net rotation of 45°. By applying a bias which depends on the frequency the total rotation is reduced to $\leq 45°$ and the peaks disappear. Second, since the birefringence changes during the switching it might cause the transmission to peak also at a certain time depending on the cell thickness and the wavelength according to Equation 4.

Another interesting feature which appears for large voltages is an asymmetry in the response. This is seen as a difference in the rise and fall responses and also in the shape of the response curves. We suggest two reasons for this behavior: 1) Asymmetry in the surface conditions of the two boundaries which causes the structure to switch differently in the two directions, i.e., the two unwound states have different elastic energy minima. 2) As the helix is unwound a net macroscopic polarization appears and the behavior resembles that of the SSFLC. Therefore a hysteresis and domains appear. Because of reason (1) this hysteresis is assymmetric

in the response. We have found that the assymmetry may be suppressed by applying a dc bias, as one would expect for the condition of an assymmetric hystersis. These properties of the switching behavior should be studied in more depth, both from the viewpoint of device operation and the physics involved.

The response from an OASLM which incorporates the CS-1017 mixture is shown in Figure 4. For 5 μm thick cells, as in the case of the electrically addressed SLM described above, the LC structure is helicoidal. This was determined by the appearance of dark stripes under the microcope and a diffraction pattern which disappeared with an applied voltage greater than the unwinding voltage. LCs having a thickness of 5 μm do not function well in an OASLM, probably because their capacitance becomes too low compared to the *a*-Si:H photosensor capacitance.[2,4] Therefore the device of Figure 4 has a 3 μm thick LC. It is not sufficiently thick to permit a pure, undistorted helix to exist in a mixture having this pitch, which is larger than that of FLC-6200; the helix, if it exists at all, is distorted by the surfaces even in the absence of a field. There is no orientation of the cell which produces an extinction in the transmittance of monochromatic light with this sample at zero voltage, indicating a nonuniformity exists, probably with a splay of the molecular director in the direction perpendicular to the glass plates.[24] The figure demonstrates the ability of these structures, which exhibit neither a pure helix nor a perfect SSFLC structure, to modulate light. The output read-light intensity versus the write-light intensity exhibits a linear and continuous dependence up to 0.2 mW/

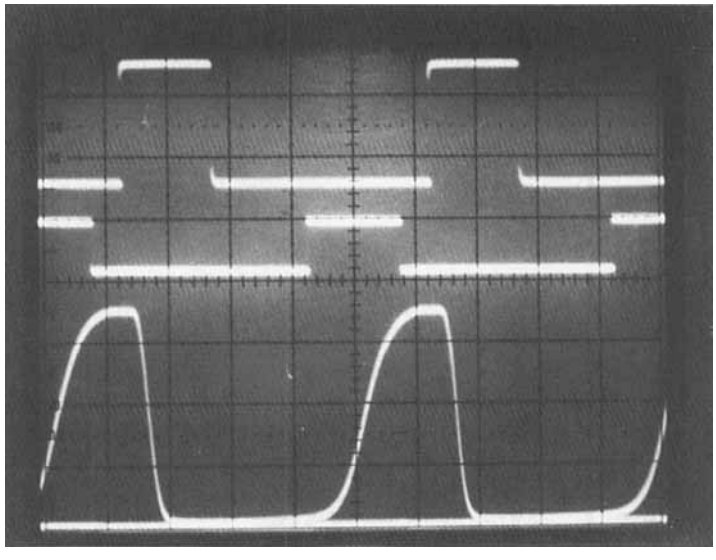

FIGURE 4 Oscilloscope traces to show the response of a 3 μm thick DHF-OASLM made with CS-1017 liquid crystal mixture. The upper trace shows the applied square pulses with 1 kHz repetition rate at 30 volts peak-to-peak with 10.5 volts dc bias. The central trace shows the positions of the write-light pulses from the Ar+ laser (5 mW/cm^2) during the negative-bias interval with a 300 μs pulse width. The bottom trace is the response of the device showing a contrast ratio of >70:1, a rise time of 225 μs, a delay time of 100 μs and a fall time of 60 μs. (Note: Optimal resolution is usually found at lower write-light intensities, for which the contrast ratio is lower.)

cm^2 and then saturates. When this device was read with a white light it appeared blue in the OFF state and pink in the ON state. When a spatially varying pattern was written on the device, the areas which were ON appeared pink, with the remaining area appearing blue.

To demonstrate a DHF-OASLM with a pure, undistorted helicoidal structure we used the Hoffman-La Roche mixture FLC-6200, which has a pitch of 0.37 μm at room temperature. The response of a 2.4 μm thick OASLM is shown in Figure 5. It exhibits a contrast ratio of 30:1 in the saturated state. The response is linear with the write-light intensity up to 1 mW/cm^2 and it switches with a response time of 250 μs. The fact that the linear range is larger with the FLC-6200 cell than the 3 μm cell made of CS-1017 is probably due to the fact that the polarization of FLC6200 is 100 nC/cm^2 while that for CS-1017 is 10 nC/cm^2, since higher polarization requires higher switching energy. The color selecting capability was shown in a previous paper.[14] The reflected read light is dark in the OFF state, and then it switches to blue at low write-light intensities which becomes brighter continuously as the intensity increases. Above a certain write-light intensity yellow-green domains start to appear which grow until the whole irradiated area switches to yellow-green for a write-light intensity of 3–4 mW/cm^2. By imaging a resolution target onto the photosensor the resolution was found to be 28 lp/mm. A detailed discussion on the origin of the color is given in the next section.

VI. SLMs RESPONSE TIME

The behavior of the switching speed of the DHF devices with the voltage is shown in Figure 6. The response time at low fields is in the ms range and has no field

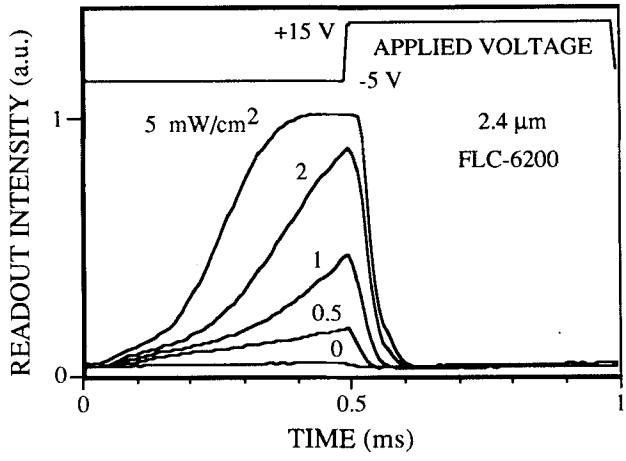

FIGURE 5 Oscilloscope traces showing the response of a 2.4 μm thick DHF-OASLM incorporating Hoffman-La Roche mixture FLC-6200. The upper trace shows the 1 kHz applied square wave voltage with 20 volts peak-to-peak and 5 volts dc bias. The write light in this case was continuous. The response of the device is shown here at different write light intensities as indicated.

dependence. This agrees with the approximate solution given in Equations 2 and 3. For larger fields the switching times start to decrease.

According to numerical solutions[17] of the dynamic Equation 1, the switching time should decrease like $\tau \sim 1/E$ for intermediate fields and like $\tau \sim 1/\sqrt{E}$ for high electric fields. Our qualitative understanding of this switching-time behavior with field in the three regions is as follows: In the small-field region the structure is distorted slightly but the average polarization is still zero and therefore the switching has relaxation-type behavior. Therefore the switching time in this case is determined by the elastic relaxation time which has no field dependence. At intermediate fields a net polarization density starts to appear which, when coupled to the electric field, causes the switching to be similar to the SSFLC case where $\tau \sim 1/E$. In the large fields regime where the walls which formed between the planes at $\varphi = \pi, 3\pi, 5\pi, \ldots$, for $E > 0$ and between the planes at $\varphi = 0, 2\pi, 4\pi, \ldots$, for $E < 0$ start to shrink with a solitary wave behavior. The speed of this sine-Gordon soliton behaves[17,25] like $\sqrt{E}$ and therefore $\tau \sim 1/\sqrt{E}$.

The behavior in Figure 6 resembles this general behavior. The differences could be a result of nonidealities in the structure. The one dimensional helix switching described by Equation 1 does not include surface interactions. These are known to have strong influence on the helix of planar samples and make the structure two dimensional with defects such as disinclination lines.[21,24] Cells prepared with different surface conditions exhibited switching speed behavior different from the one shown in Figure 6, particularly in the high field limit. For device operation the main point is that the switching speed is in the 100 μs range. For analog response

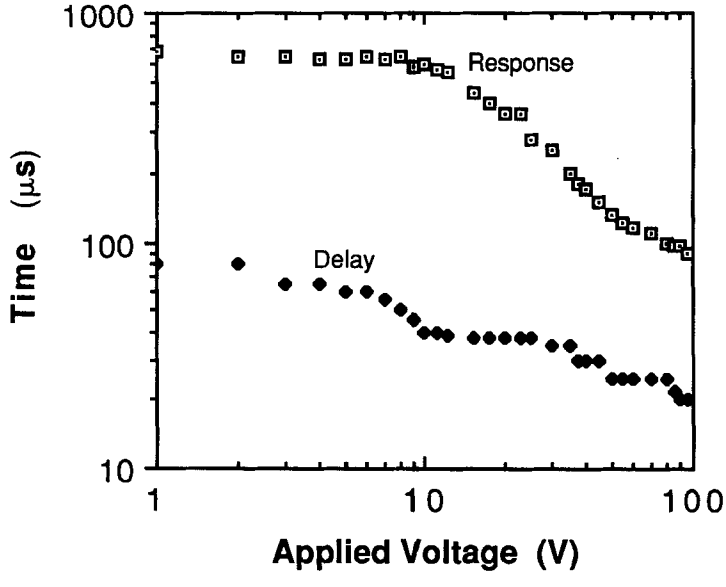

FIGURE 6 The optical response time (0–90%) and delay time (0–10%) versus the peak voltage of the applied clock positive square-wave pulses with a frequency of 400 Hz. The sample and the geometry are the same as in Figure 3.

operation, however, one needs to operate at low fields or, when the applied field is ac, at low-to-intermediate fields. The reason that the analog range is extended for ac is that the LC does not have time to saturate during each voltage half-period.

VII. COLOR SELECTING CAPABILITY

The color of the read out light in the DHF-SLMs is a function of several parameters. The parameters change with the polarizer-analyzer orientation and the relative cell orientation. When applying an ac voltage, the color changes with the amplitude, the bias, and the frequency. When looking at the cells without polarizers, they appear colored with the color changing as a function of viewing angle. These latter colors are a result of the selective reflection of light from the helicoidal structure when the light propagates with a finite angle to it.[20] This selective reflection is not the subject of the present paper. Here we are dealing with the case of light propagating perpendicular to the helix. The optical properties in this case were described analytically in Section III.

In order to quantify the color changes and to understand their origin, we performed spectral measurements on an electrically addressed cell incorporating CS-1017 LC. Figure 7 shows transmittance through the cell between crossed polarizers with the cell oriented such that near-extinction observed with no applied voltages,

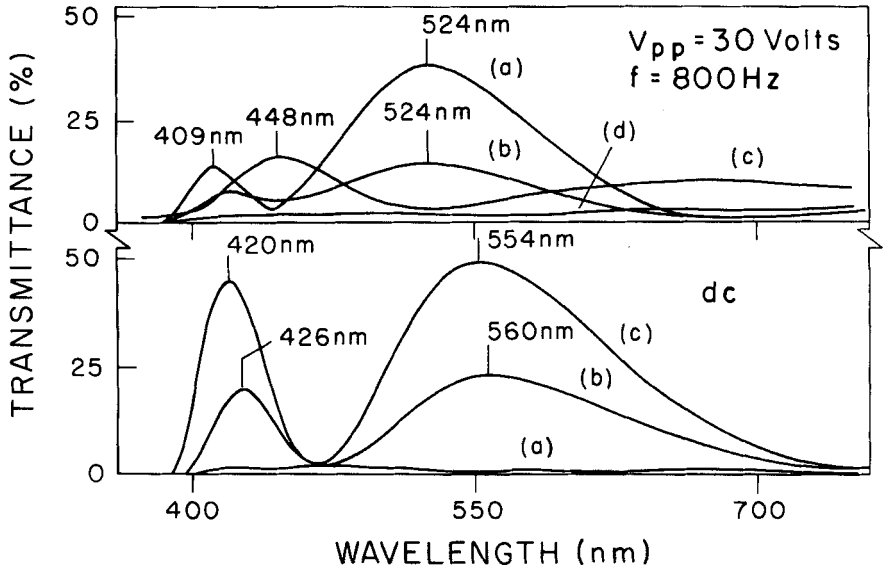

FIGURE 7 Transmittance versus wavelength for the sample of Figure 3 between crossed polarizers. The sample was oriented such that near-extinction is seen with no applied voltage. The lower curves correspond to different dc applied voltages: (a) 0 volts (b) 4 volts and (c) 10 volts. The upper curves correspond to an 800 Hz square wave voltage with 30 volts peak-to-peak and different dc biases (a) 0 volts (b) 4 volts (c) 6 volts and (d) 10 volts.

as seen in curve (a) of the lower part. With increasing the voltage two birefringence peaks appear within the visible range of the spectrum. The peaks have their positions at wavelengths where the half waveplate condition is satisfied: $\lambda = 2d\Delta n/(2m + 1)$ where $m = 0, 1, 2, \ldots$. The peaks heights are determined by the rotation of the optic axis according to Equation 4. By measuring the transmittance of unpolarized light through the cell, interference fringes due to reflections from the boundaries were observed. From the separation of these fringes we estimated the sample thickness to be $d = 5.6$ μm. The average refractive index of the LC seen by unpolarized light was taken as $n_{avg} = 1.6$. With this value of d we deduced that the birefringence peaks in the neighborhood of 500 nm correspond to $m = 1$ in the above-mentioned half-wave plate condition. The shorter wavelength peaks correspond to $m = 2$. This way the birefringence was estimated as a function of the different parameters from the shift of the $m = 1$ peak position. The shorter wavelength peaks have slightly lower heights than the $m = 1$ peaks. We explain this as a result of higher absorption of the LC material and the polarizers in the shorter wavelength region. Since we are not presently concerned with the absolute

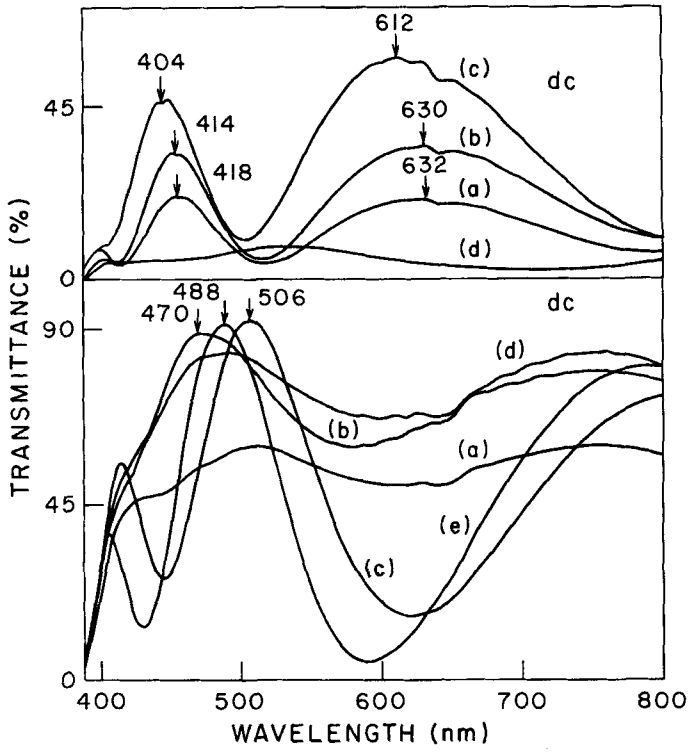

FIGURE 8 Transmittance versus wavelength at different dc voltages for the sample of Figure 3 but with the sample rotated 80° from its orientation of Figure 7. The lower curves correspond to the sample between parallel polarizers under different dc applied voltages: (a) 0 volts (b) −2.5 volts (c) −2 volts (d) −10 volts and (e) +10 volts. The upper curves correspond to the sample between crossed polarizers under: (a) 0 volts (b) −1.5 volts (c) −10 volts and (d) +10 volts.

value of the transmitted light we shall not pursue this further here. The curves in the upper part of Figure 7 correspond to the same geometry but the driving voltage is a square wave with a frequency of 800 Hz and a peak-to-peak voltage of 30 volts. The different curves correspond to different dc bias voltages. With no bias the transmission corresponds to that from the two unwound states (V_+ and V_- are larger than the unwinding voltage V_c). The $m = 1$ peak is wide and peaks at 524 nm. The ratio of $m = 2$ peaks heights to $m = 1$ peaks heights is much smaller compared to that in the lower part of Figure 7. This additional decrease is possibly due to scattering[26] from domains during the switching, which is enhanced at shorter wavelengths. Therefore the color in this case is green-yellow, which was confirmed by looking at the cell under the microscope. As the bias increases the transmission corresponds to that from one unwound state (corresponding to a positive voltage V_+) plus that of the other state which corresponds to V_-. If $V_- < V_c$ this latter state will cause the peaks to shift and their heights to drop. In curve (*c*) the $m = 1$ peak is positioned at 448 nm, i.e., the sample color has switched to violet-blue. With 10 volts bias [curve (*d*)] the cell becomes dark. The changes in the color with

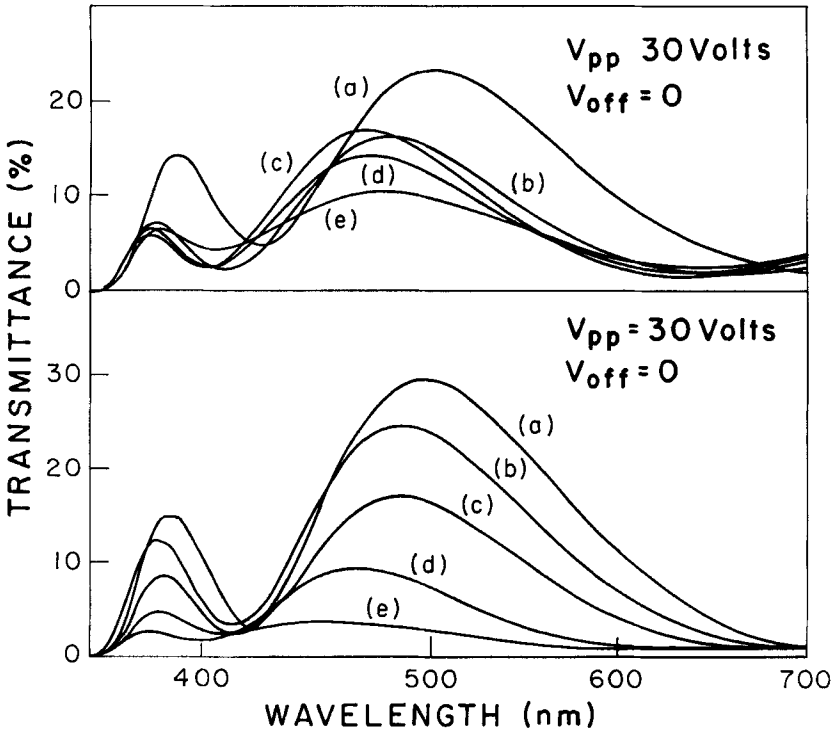

FIGURE 9 Transmittance versus wavelength for the sample of Figure 3 between crossed polarizers at different frequencies of a 30 volts peak-to-peak square wave voltage. The lower curves correspond to orientation of the cell such that extinction is seen with no applied voltage: (a) 100 Hz (b) 200 Hz (c) 300 Hz (d) 800 Hz and (e) 1600 Hz. The upper curves correspond to 20° orientation of the cell from the previous position: (a) 100 Hz (b) 400 Hz (c) 800 Hz (d) 1100 Hz and (e) 1600 Hz.

offset are important in explaining the color changes in a DHF OASLM with write-light intensity because the V_- which drops across the LC increases with the write-light intensity.

Examples of spectral variations with applied voltage which correspond to different polarizer-analyzer and sample orientations are shown in Figure 8. The lower curve shows that, for the cell between parallel polarizers, the color changes from white to pink to green-violet to blue-violet by changing the voltage gradually from -10 V to 10 V. The upper part shows that the $m = 1$ peak falls in the red region compared to the lower part of Figure 7 for a different orientation of the cell between crossed polarizers, and that color changes are more pronounced in this position.

Examples of spectral variations with the frequency are shown in Figure 9. These changes are consistent with the color changes observed under the microscope when changing the frequency.

VIII. ORIGIN OF THE COLOR CHANGES

The results in the previous section demonstrate that the shifts in the birefringence peaks positions correspond to the color changes. Associated with that are the changes in their heights and widths. To determine the exact color that each of these curves represents one needs to follow the procedure of assigning positions for each on a CIE chromaticity diagram.

To prove that these changes are due to changes in the birefringence and the optic axis rotation we compared the estimated birefringence from the $m = 1$ peak positions and the axis rotation to calculated values. We carefully measured the wavelength of the peak position and the average optic axis direction α by looking at the orientations of the cell which produced an extinction in the transmittance. For square-wave applied voltages, α was measured by measuring the amount of rotation of the cell required to give maximum output during V_+ and V_- states, and dividing by two. In Figures 10, 12, and 13 we show all of these values as a function of the dc voltage, the peak voltage of 1 kHz square wave, and the frequency, respectively.

For the calculated birefringence we used the average of the expression in Equation 6 for $n_e(z)$, which may be approximated as:

$$n_e(z) \approx \sqrt{\varepsilon_\parallel}\left(1 - \frac{\delta\varepsilon}{2\varepsilon_\perp}\sin^2\theta \sin^2\varphi\right) \tag{14}$$

The average is determined by the average $\langle\sin^2\varphi\rangle$ where $\langle\ \rangle$ denotes space average over one period. In terms of the angle Ω (Equation 5) which the molecular axis projection on the yz plane makes with the z axis this average is given by:

$$\langle\sin^2\varphi\rangle = 1 - \frac{1}{\tan^2\theta}\langle\tan^2\Omega\rangle \tag{15}$$

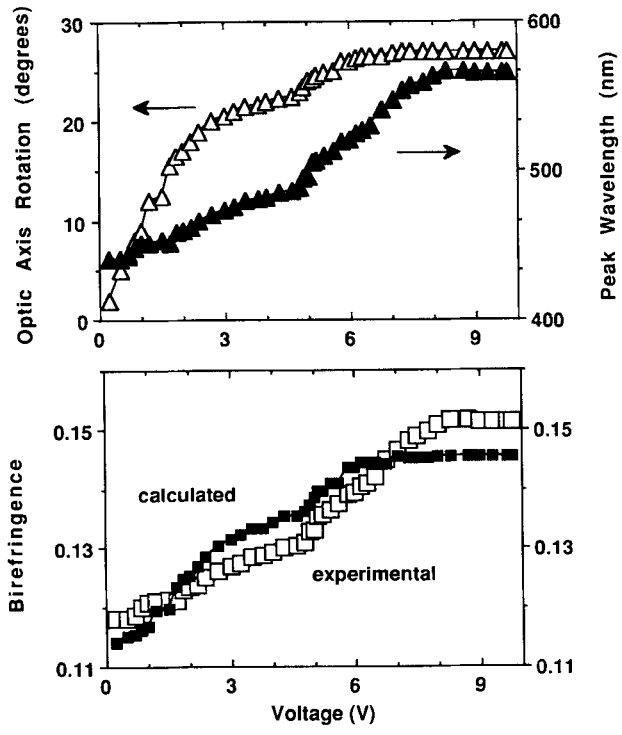

FIGURE 10 Upper: the measured optic axis rotation (left) and the birefringence peak wavelength (right) versus the dc voltage on the cell of Figure 3. Bottom: the experimental and calculated birefringence versus the applied dc voltage.

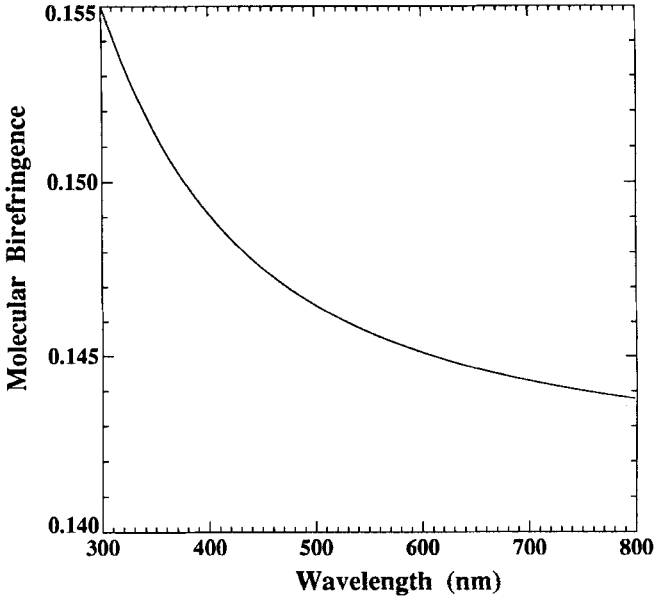

FIGURE 11 Dispersion of the molecular birefringence, used in calculating the effective average birefringence.

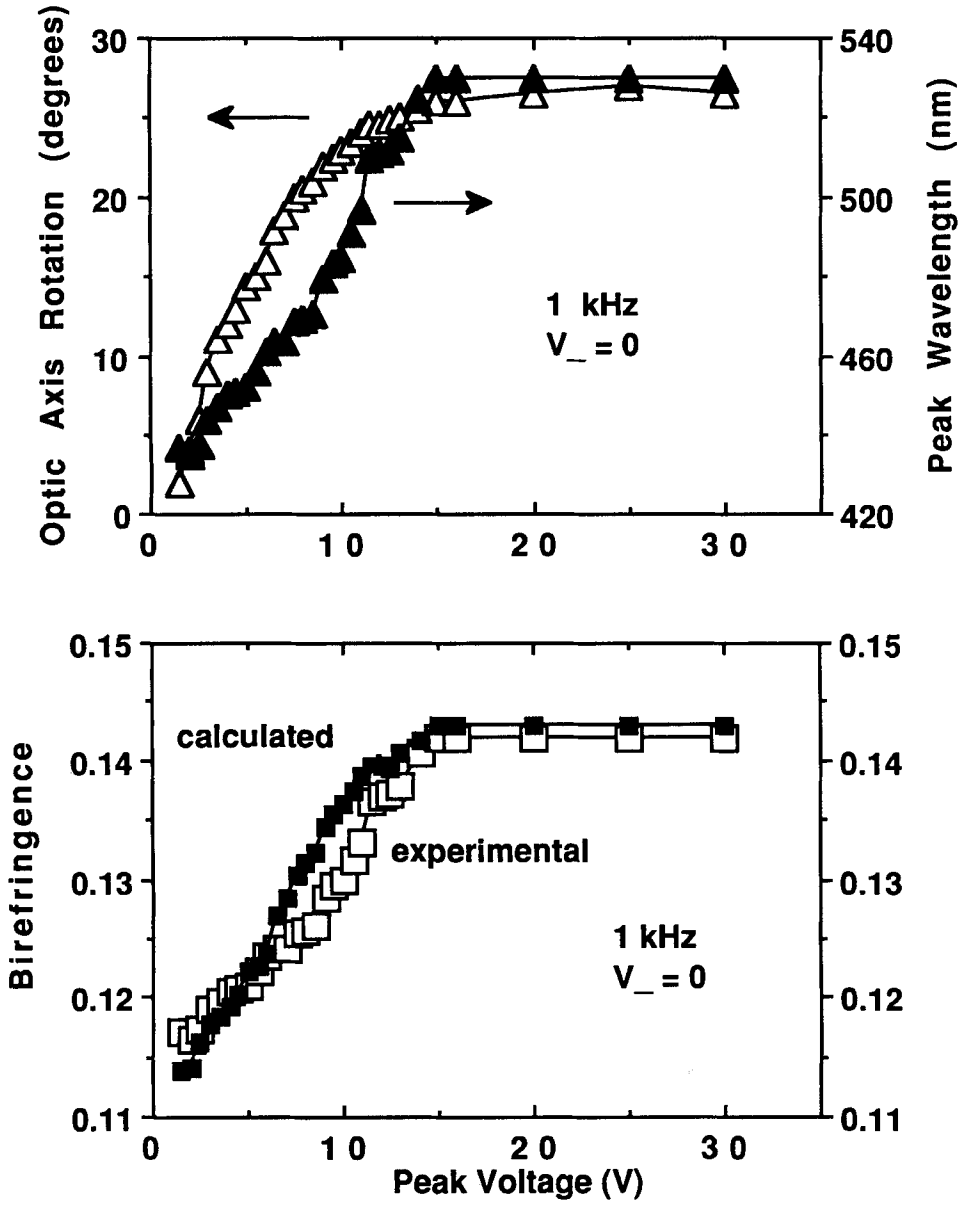

FIGURE 12 Upper: the measured optic axis rotation (left) and the birefringence peak wavelength (right) versus the peak voltage of a 1 kHz positive square wave pulses on the cell of Figure 3. Bottom: the experimental and calculated birefringence versus the peak voltage.

The average $\langle \tan^2\Omega \rangle$ is simply determined from the measured average optic axis direction α, that is $\langle \tan^2\Omega \rangle = \tan^2\alpha$. Therefore the average $\langle n_e(z) \rangle$ is calculated by inserting expression (15) in place of $\sin^2\varphi$ in Equation 6. In this sense the calculated birefringence is a semi-theoretical calculation because it is based on the measured

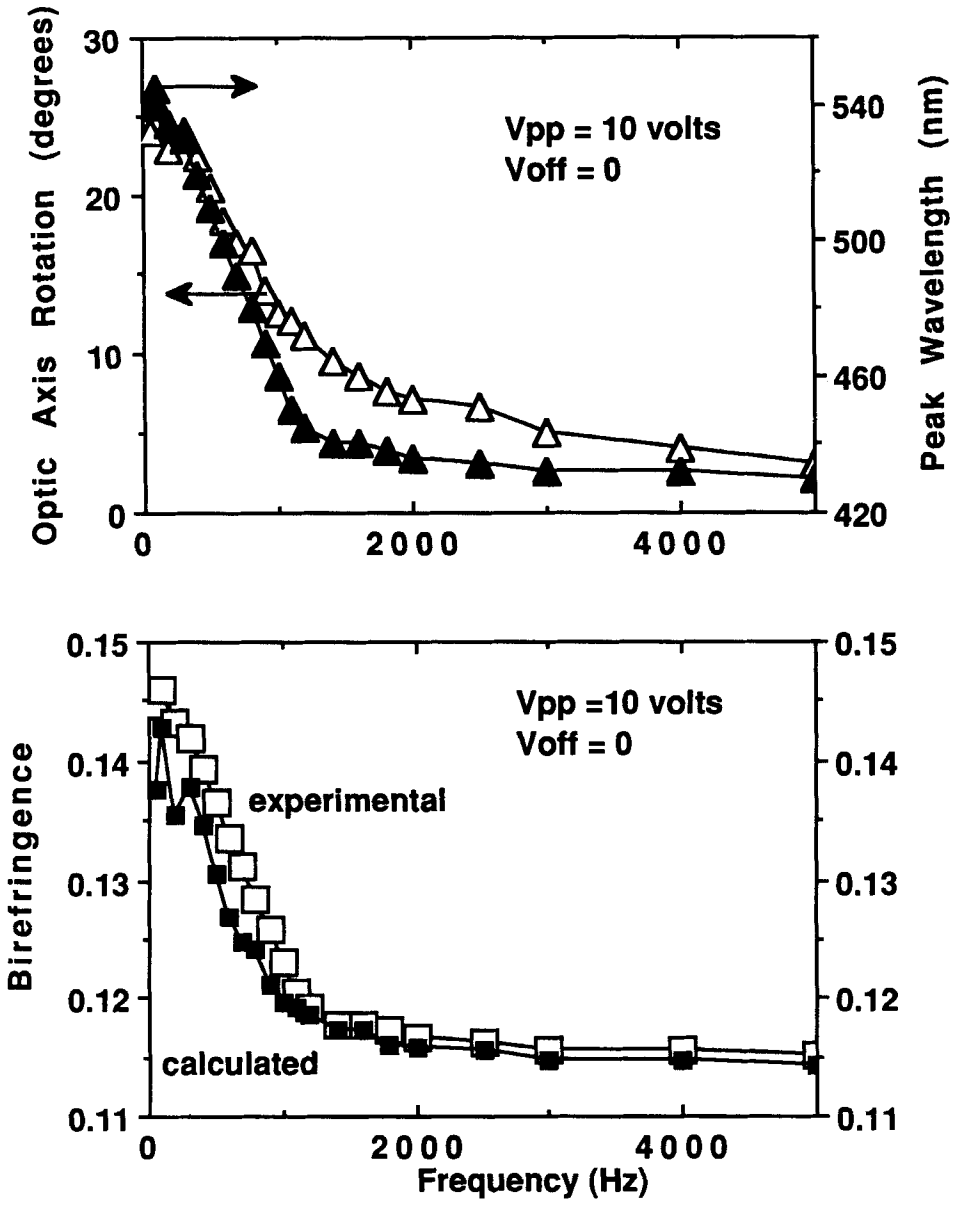

FIGURE 13 Upper: the measured optic axis rotation (left) and the birefringence peak wavelength (right) versus the frequency of a 10 volts peak-to-peak square wave with no bias on the cell of Figure 3. Bottom: the experimental and calculated birefringence versus the frequency.

optic axis rotation α. A pure theoretical calculation would be either to perform the averaging numerically or to use an analytic solution similar to the one we derived in Equation 13. However, this expression is valid only for small distortions. The quadratic behavior expected from Equation 13 is seen in Figures 10, 12, and

13 in the small distortion region. A straightforward calculation of Δn_{avg} from Equation 13 shows that it agrees quantitatively with the measured values up to $\Delta n_{avg} \approx 0.125$. Another important fact from these figures is that α changes linearly with the voltage for the case of small voltages in agreement with Equation 12. From Figure 9 the slope of the linear part is ~9 degrees/volt which when compared to that from Equation 12 yields $E_c = 0.17$ volts/μm in agreement with the expected value of $E_c = 0.2$ volts/μm for CS-1017 LC as estimated from the diffraction measurements. Therefore Equation 12 provides us with a simple way to measure E_c.

Dispersion of the molecular birefringence was taken into consideration in calculating the average birefringence. Wu's dispersion formulae[27] for the molecular birefringence of LCs is not suitable for our purposes because we need the dispersion of $\varepsilon_\perp$ and $\varepsilon_\parallel$ separately for Equation 6. For this purpose we followed a procedure similar to that used by Wu to derive our own dispersion formulae for $\varepsilon_\perp$ and $\varepsilon_\parallel$. It consists of solving Vuks's equation,[28] which relates the molecular polarizability to the indices of refraction $n_\perp$ and $n_\parallel$ (details of the calculation will be published elsewhere).[29] The calculated dispersion curve of the molecular birefringence used in the calculation of the average effective birefringence is given in Figure 11. It shows a weak dispersion so that it does not account for the observed shifts of the transmittance peaks.

The calculated and measured average birefringence values agree to within 10% as seen in Figures 10, 12, and 13. This indicates the validity of our approach and supports our proposition that the shifts in the birefringence peaks are a result of changes in the birefringence which causes the color changes. This also holds for an applied voltage which is an ac square wave and its frequency dependence (Figure 12). As the frequency changes, the unwinding voltage changes and with it the average optic axis direction and the average birefringence. This fact is clear for small distortions from Equation 12 and Equation 13. Therefore we conclude that the color changes as function of frequency are due to changes in the averaged optic axis direction and averaged birefringence and not due to temporal averaging effect of the human eye or a slow response of the spectrometer as previously reported by Beresnev *et al.*[12]

IX. CONCLUSIONS

We have studied the electro-optic effects associated with the helix distortion of ferroelectric liquid crystals and their application to light modulation and color switching. Approximate analytic expressions for the average optic axis direction and the birefringence were derived for the case of small distortions. We showed that this rotation is linear with the applied field while the birefringence changes are quadratic. The rotation of the optic axis was shown to be in a plane allowing for large viewing angles when the DHF-SLMs used for displays. These expressions also explain the analog response of the DHF-SLMs at low fields. From the slope of the rotation angle of the optic axis versus the field we found an easy way to determine the unwinding field.

Spatial light modulators based on the helix distortion having different thicknesses were demonstrated. Optically addressed SLMs with hydrogenated amorphous silicon photodiode as the photosensor exhibit an analog response with color selecting capability, high contrast ratio, high resolution, and short response time. The applicability of cells having their structure in between a perfect helicoid and surface stabilized structure to light modulation was demonstrated. These cells exhibit output characteristics similar to the ones with the perfect helix, but in addition the off state is also colored.

Changes in color as a function of the applied voltage, bias and frequency result from the shifts of the transmittance spectral peak positions and changes in their heights. The measured birefringence values estimated from the maximum transmission peaks positions agree to within 10% with the calculated birefringence. To account for the dispersion of the optical dielectric constants we derived a dispersion formulae for them based on Vuks's relation.

From the agreement between measured and calculated birefringence it appears that color changes are due solely to birefringence changes and the averaged optic axis rotation and the dispersion which are associated with them.

Acknowledgements

We are grateful to Dr. J. Funfschilling from Hoffman-La Roche for providing the FLC-6200 LC mixture. The cooperation of B. Landreth in performing part of the experiments and his comments on the manuscript are highly appreciated. We also benefited from discussions with Profs. N. Clark and D. Walba. This work was supported by the National Science Foundation Engineering Research Center grant No. CDR-862236.

References

1. See for example, L. M. Blinov, Electro-optical and Magneto-optical Effects of Liquid Crystals, (Wiley, New York, 1983).
2. G. Moddel, "Optically Addressed Spatial Light Modulators," in Physics and Applications of Amorphous and Microcrystalline Semiconductor Devices, J. Kanicki, editor, Norwood, MA, Ch. 13, in press.
3. N. A. Clark and S. Lagerwall, *Appl. Phys. Lett.*, **36**, 899 (1980).
4. G. Moddel, K. M. Johnson, W. Li, R. A. Rice, L. A. Pagano-Stauffer and M. A. Handschy, *Appl. Phys. Lett.*, **55**, 537 (1989); W. Li, R. A. Rice, G. Moddel, L. A. Pagano-Stauffer and M. A. Handschy, *IEEE Trans. Elect. Devices*, **36** (12), 2959 (1989).
5. S. Garoff and R. B. Meyer, *Phys. Rev. Lett.*, **38**, 848 (1977); Phys. Rev. A 19, 338 (1979).
6. G. Andersson, I. Dahl, P. Keller, W. Kuczynski, S. T. Lagerwall, S. Skarp and B. Stebler, *Appl. Phys. Lett.*, **51**, 640 (1987).
7. I. Abdulhalim, G. Moddel and K. M. Johnson, *Appl. Phys. Lett.*, **55**, 1603 (1989); I. Abdulhalim, G. Moddel, K. M. Johnson and C. M. Walker, *J. Non. Cryst. Solids*, **115**, 162 (1989).
8. R. B. Meyer, L. Liebert, L. Strzelecki and P. Keller, *J. de Physique Lett.*, **36**, L-69 (1975); R. B. Meyer, *Mol. Crys. Liq. Cryst.*, **40**, 33 (1977).
9. B. I. Ostrovskii and V. G. Chigrinov, *Sov. Phys. Crystallogr.*, **25**, 322 (1980); B. I. Ostrovskii, A. Z. Rabinovich and V. G. Chigrinov, in "Advances in Liquid Crystal Research and Applications," Edited by Lajos Bata, Pergamon Press, Oxford, 1980, pp. 469.
10. L. A. Beresnev, L. M. Blinov, D. I. Dergachev, A. I. Zhindulis, I. S. Klimenko, S. I. Padea and A. A. Sargeev, *Sov. Tech. Phys. Lett.*, **14**, 117 (1988).
11. L. A. Beresnev, V. G. Chigrinov, D. I. Dergachev, E. P. Poshidaev, J. Funfchilling and M. Schadt, *Liq. Cryst.*, **5**, 1171 (1989).

12. L. A. Beresnev, L. M. Blinov and D. I. Dergachev, *Ferroelectrics*, **85**, 173 (1988), and **92**, 335 (1989).
13. J. Funfchilling and M. Schadt, *J. Appl. Phys.*, **66**, 3877 (1989), and *SID Digest of Technical Papers*, **21**, 106 (1990).
14. I. Abdulhalim, B. Landreth and G. Moddel, *SID Digest of Technical Papers*, **21**, 330 (1990).
15. B. Landreth, C. C. Mao, I. Abdulhalim and G. Moddel, to be published.
16. J. E. Maclennan, M. A. Handschay and N. A. Clark, *Phys. Rev.*, **A34**, 3554 (1986).
17. J. E. Maclennan, Ph.D. thesis, University of Colorado at Boulder, 1988.
18. B. I. Ostrovskii, S. A. Pikin and V. G. Chigrinov, *Sov. Phys. JETP*, **50**, 811 (1979).
19. V. E. Dmitrienko and V. A. Belyakov, *Sov. Phys. JETP*, **51**, 787 (1980).
20. I. Abdulhalim, L. Benguigui and R. Weil, *J. de Physique*, **46**, 815 and 1429 (1985); I. Abdulhalim, *Opt. Commun.*, **64**, 443 (1987).
21. M. Glogarova and J. Pavel, *J. de Physique*, **45**, 143 (1984).
22. I. Abdulhalim *et al.*, to be published.
23. M. A. Handschay and N. A. Clark, *Ferroelectrics*, **59**, 69 (1984).
24. J. Pavel, *J. de Physique*, **45**, 137 (1984).
25. P. E. Cladis, H. R. Brand and P. L. Finn, *Phys. Rev.*, **A28**, 512 (1983).
26. K. Yoshino and M. Ozaki, *Ferroelectrics*, **59**, 145 (1984).
27. S. T. Wu, *Phys. Rev.*, **A33**, 1270 (1986).
28. M. F. Vuks, *Opt. Spectros.*, **20**, 361 (1966).
29. I. Abdulhalim, *Mol. Crys. Liq. Cryst. Lett.*, in press.